PCCP

PAPER

View Article Online
View Journal

Cite this: DOI: 10.1039/d6cp00935b

Revisiting the intersystem crossing mechanisms in chromophore dimers through the lens of excitonic coupling: a case study of naphthalimide

Monika G. Mutovska,[a] Darío Puchán Sánchez,[b] Arthur H. G. David,[b] Clément Cabanetos,*[b] Tangui Le Bahers,[cd] Yulian Zagranyarski,*[a] Cyrille Monnereau*[c] and Josene M. Toldo*[e]

Intersystem crossing (ISC) efficiency is primarily governed by the magnitude of spin–orbit coupling, which is typically enhanced by heavy-atom effects and molecular symmetry effects. Recent studies have suggested that charge transfer and/or excitonic coupling between neighboring chromophore units, either covalently linked or spatially associated, can also play a key role in this process. Here, we demonstrate a molecular design strategy to enhance triplet generation based on excitonic coupling in covalently linked homodimers. A series of naphthalimide dimers bridged by chalcogen linkers (O, S, Se) was synthesized to systematically modulate interchromophoric electronic communication, probed by spectroscopic and theoretical investigation. Our results show that the oxygen-linked dimer (**Napht$_2$[O]**) exhibits minimal changes in absorption and emission spectra relative to the parent monomer. In contrast, **Napht$_2$[S]** and **Napht$_2$[Se]** dimers display pronounced excitonic signatures, accompanied by luminescence quenching and enhanced singlet oxygen generation, attributed to ISC enhancement. Time-dependent density functional theory calculations, combined with excitonic analysis based on transition density matrix, revealed how dimerization-induced modifications in excited-state character are crucial for maximizing ISC rates. Our findings demonstrate that increasing excitonic coupling through heavier chalcogen bridges can dramatically accelerate ISC in homodimers by inducing changes in excited-state character between singlet and triplet states, without invoking a full charge-separation step. Beyond these specific results, this work highlights excitonic coupling as a versatile handle for engineering ISC in molecular assemblies, opening new perspectives for the design of photoactive materials for optoelectronics, photocatalysis, and photodynamic applications.

Received 13th March 2026,
Accepted 30th April 2026

DOI: 10.1039/d6cp00935b

rsc.li/pccp

1. Introduction

Excited singlet-to-triplet Intersystem crossing (ISC) plays a pivotal role in a variety of applications, ranging from organic electronics to therapeutic applications.[1–6] In organic light-emitting devices, for example, molecules showing efficient and reversible singlet-to-triplet ISC can be used to improve device efficiency, which is otherwise limited by spin statistics and the forbidden character of the radiative $T_1 \rightarrow S_0$ transition.[7–9] In artificial photosynthesis or photocatalysis, intersystem crossing is essential for the generation of a long-lived excited state, enabling more efficient charge separation[10–12] and photoinduced electron or energy transfers,[13–15] respectively. In chemical biology, ISC leads to the production of various reactive oxygen species, which find potential therapeutic applications in photodynamic therapy (PDT).[16–18]

Intersystem crossing efficiency is primarily determined by two key factors: the magnitude of the spin–orbit coupling (SOC) and the energy difference between the lowest singlet excited state and the triplet manifold.[19] Different strategies can be used to improve SOC in molecules.[20,21] A classical way is introducing heavy atom substituents (such as I, Os, Pt, Ru, Ir *etc*),[22] which enhances SOC through relativistic effects, a phenomenon known as ''heavy atom effect''.[23,24] However, ISC enhanced by the heavy-atom effect often implies higher synthetic costs and can lead to dark toxicity effects in the context of PDT applications.[25]

Another way of enhancing ISC involves the change in the character of the excited states involved in the process.

[a] *Faculty of Chemistry and Pharmacy, Sofia University ''St. Kliment Ohridski'', 1 J. Baurchier blvd., 1164, Sofia, Bulgaria*
[b] *Univ Angers, CNRS, MOLTECH-ANJOU, SFR MATRIX, F-49000 Angers, France*
[c] *ENS de Lyon, CNRS, Laboratoire de Chimie UMR 5182, F-69342 Lyon, France*
[d] *Institut Universitaire de France, 5 rue Descartes, 75005 Paris, France*
[e] *Université Lyon 1, ENS de Lyon, CNRS, Laboratoire de Chimie UMR 5182, Lyon, France. E-mail: josene-maria.toldo@ens-lyon.fr*

According to El-Sayed's selection rules, which are based on orbital symmetry considerations, the forbidden nature of the ISC process can be alleviated if there is a change in the molecular orbital type during the process. Typically, molecules featuring a low-lying nπ* singlet excited states (as in aromatic ketones, such as benzophenones, quinone, or phenalenone) undergo efficient ISC to a ππ* triplet state.[26–28] However, synthesizing triplet photosensitizer molecules that operate *via* this mechanism can be challenging. Alternatively, the magnitude of SOC can be tuned by lowering molecular symmetry through distortions of the aromatic framework.[29–34] Furthermore, other less conventional mechanisms to promote ISC have also been reported, including ISC *via* higher singlet states or *via* doubly excited states in molecular dimers.[35]

Recently, a number of reports have demonstrated the possibility of using small molecular dimers (typically bodipy)[36–39] or heterodimers (bodipy/poly(hetero)aromatic)[40–43] to promote efficient ISC. In compact electron donor/acceptor dyads, where the donor and acceptor adopt a mutually orthogonal orientation, this effect is often attributed to the so-called photoinduced spin–orbital charge-transfer enhanced ISC (SOCT-ISC).[44,45] According to this model, a long-lived charge-separated state (CSS) is formed directly upon photoexcitation, and the change in orbital angular momentum accompanying charge recombination (CR) is proposed to compensate for the change in electron-spin angular moment required for ISC.[39,46] This strategy, however, usually leads to low-energy ^{3}LE or CT states, which may limit ISC. Although the presence of a CSS has been backed up by transient spectroscopic evidence in some of the depicted systems,[47] the SOCT-ISC model does not provide a fully comprehensive theoretical framework, particularly when applied to homomolecular dimers.

In covalently linked homomolecular dimers, the donor and the acceptor units of the dyad have the same structure. Upon photoexcitation, one unit can act as the donor and the other as the acceptor, promoting a symmetry-breaking charge-transfer (SBCT)-induced ISC.[35,48] In this scenario, the molecular symmetry is disrupted, resulting in a high energy CT state with the hole (cation) and the electron (anion) localized in different units. Since the chromophore units usually adopt an orthogonal geometry, SBCT-ISC can be considered as a special case of the SOCT-ISC.[6,49,50] Furthermore, given that the donor and the acceptor are structurally equivalent, the same structural unit, the energy of the CT state tends to be higher than in conventional SOCT-ISC systems. Despite its mechanistic appeal, examples of molecules showing SBCT-ISC and efficient ISC are still scarce. Notably, a few examples involving naphthalimide dimers and derivatives were recently reported by Jing *et al.*[49] and Tian *et al.*[51] Yet, the fundamental aspects at the molecular level underlying SBCT-ISC in such systems are not fully understood.

In a recent work, we explored the concept of dimerization-induced intersystem-crossing in homomolecular dimers of benzothioxanthene imide (BTI) derivatives.[52] Combining experimental and theoretical efforts, we reported a remarkable ISC efficiency in a series of BTI dimers covalently or supramolecularly linked. The observed efficiency was found to dynamically depend on the angular orientation between the two dimer subunits (referred as through-space excitonic coupling). In the present work, we extend these concepts and propose that SOCT-ISC could also be envisioned in the framework of the classical excitonic model, with the bound electron–hole pair becoming delocalized over the two chromophore units, giving rise to mixed charge-resonant excitonic states.[53] Within this picture, excitonic coupling generates a new subset of singlet and triplet excited states, featuring partial or complete delocalization of the excitation across both subunits.

To that end, we synthesized and characterized a series of naphthalimide dimers interconnected through a chalcogen linker at their 4-carbon position (Fig. 1). We show that when oxygen is used as a linker (**Napht$_2$[O]**), the position of the absorption and emission maxima of the naphthalimide dimer remains nearly unchanged compared to the monomeric reference compound **Napht[O]Me**. In contrast, the sulfur (**Napht$_2$[S]**) and selenium (**Napht$_2$[Se]**) analogs exhibit a clear Davydov splitting of their absorption spectrum and redshift of the emission characteristic of excitonic coupling. Remarkably, these features are accompanied by an almost complete quenching of luminescence and a concomitant rise in the singlet oxygen quantum yield, suggesting that excitonic coupling between the two covalently linked fluorophores facilitates ISC. This hypothesis is backed up by time-dependent density functional theory (TDDFT) calculations and, in particular, by transition density matrix (1TDM) analyses, which confirm that excitonic and charge transfer interactions play a central role

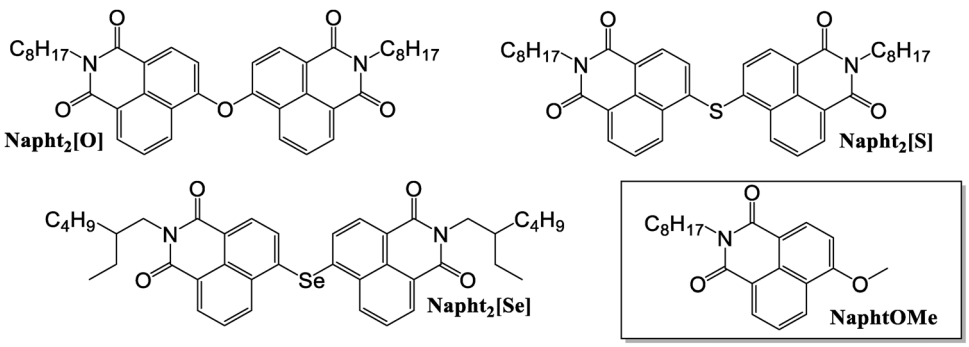

Fig. 1 Structure of the three dyes investigated in the present study, **Napht$_2$[X]** (X = O, S, Se), along with reference monomeric compound **NaphtOMe**.

in enabling efficient ISC in these metal-free small organic molecules.

2. Results and discussion

2.1. Synthesis

The synthesis of the naphthalimide dimers **Napht$_2$[O]**, **Napht$_2$[S]**, and **Napht$_2$[Se]** is depicted in Scheme 1. For all three target compounds, our approach is based on nucleophilic aromatic substitutions, initially forming the phenolate anions and the corresponding sulfur and selenium analogs. The resulting anionic forms rapidly react with the corresponding dimer.

Regarding the **Napht$_2$[O]** dimer, it was readily prepared in one step from 4-bromo-1,8-naphthalimide **1a** upon interaction with water, in the presence of cesium fluoride, in DMSO. In this case, several stepwise reactions take place: *Halex* reaction to 4-fluoro-1,8-naphthalimide, conversion to phenolate, and rapid dimerization. Despite many successive reactions, the reaction proceeded smoothly and in a moderate yield of 53% on a gram scale. This was considered satisfactory regarding the successive reactions taking place *in situ*, as described above. Increasing the amount of water and base did not affect the rate and yield of the reaction.

Excess sodium sulfide hydrate was used as the nucleophile for the synthesis of the sulfur analog **Napht$_2$[S]**. The higher nucleophilicity of the sulfide anion allows the reaction to be carried out at lower temperature. Following workup of the reaction and purification by column chromatography, the **Napht$_2$[S]** dimer was isolated in 49% yield on a gram scale, comparable to **Napht$_2$[O]**.

A similar strategy was used for the synthesis of **Napht$_2$[Se]**. Due to solubility issues of the target compound when using naphthalimide **1a** as a starting reactant, analog**1b**, bearing a 2-ethylhexyl in place of the octyl substituent on the nitrogen, was synthesized. This modification was later confirmed not to significantly affect the spectroscopic or photophysical properties of **Napht$_2$[Se]**. Compound **1b** reacted smoothly with a solution of previously prepared disodium diselenide in dry NMP. The reaction proceeded rapidly in 1 h at 90 °C. After workup and purification by column chromatography, the **Napht$_2$[Se]** dimer was isolated in 61% yield, which is comparable to the yields obtained for the other two dimers. Detailed synthetic procedures, along with NMR (Fig. S1–S7) and HRMS (Fig. S8–S10) are provided in the SI.

2.2. Spectroscopy

All spectra were recorded in chloroform, in *ca.* 5×10^{-5} mol L^{-1} concentration for the absorption spectra and molar extinction coefficient determination, and 2–5 $\times$ 10^{-6} mol L^{-1} for emission spectroscopy. The main spectroscopic features are summarized in Table 1 and illustrated in Fig. 2, which shows the absorption and normalized emission spectra recorded for **Napht$_2$[O]**, **Napht$_2$[S]**, and **Napht$_2$[Se]**. This figure also displays the computed spectra for the three molecules obtained using the nuclear ensemble approach (NEA) based on a Wigner distribution of the corresponding minima.[54] Although the calculated spectra exhibit a systematic blueshift relative to the experimental spectra, all the key spectral features and overall patterns are well reproduced. The shift in the computed spectra mainly reflects limitations of the underlying electronic-structure method used to compute excitation energies. The NEA approach is primarily intended to reproduce spectral band shapes, relative intensities, and vibronic broadening through thermal sampling of nuclear geometries, rather than using a single geometry to broaden the absorption spectrum (typically, band maxima are redshifted relative to the vertical excitation by an average of 0.11 eV).[55] Individual absorption, emission, and phosphorescence spectra (recorded at 77 K) are provided in the SI Fig. S11.

The absorption spectrum of **Napht$_2$[O]** is dominated by a main band peaking in the UV (λ_{abs} = 360 nm), with an onset near 400 nm. This band shows a clear vibronic progression, characteristic of a localized $\pi\pi^*$ excited state (LE), as confirmed by quantum chemical calculations discussed later. Molar extinction

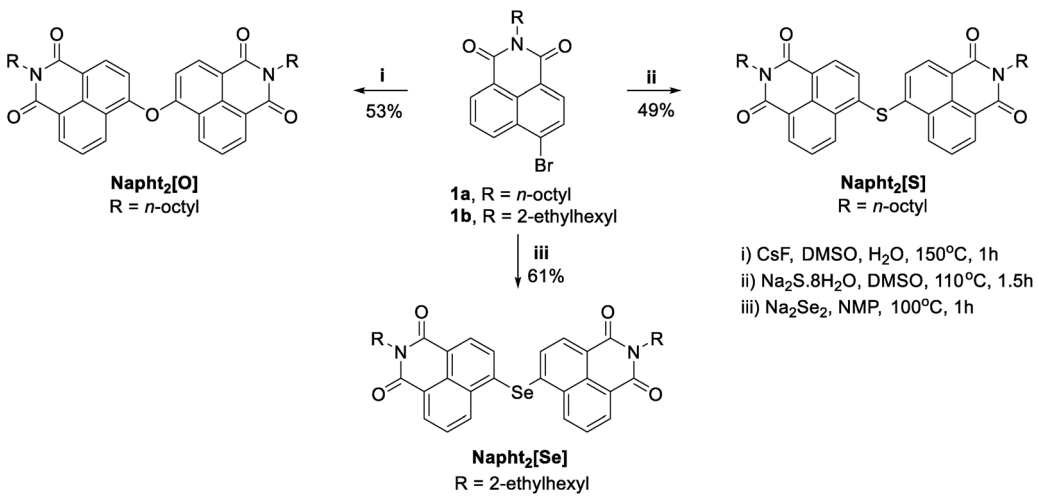

Scheme 1 Synthesis of the naphthalimide dimers **Napht$_2$[O]**, **Napht$_2$[S]**, and **Napht$_2$[Se]**.

Table 1 Main spectroscopic features of studied compounds

Compound	λ_{abs} (nm)[a]	λ_{em} (nm)[a]	φ_f[ab]	φ_Δ[ac]	τ_f (ns)[ad]	Stoke's shift (cm^{-1})
Napht$_2$[O]	362	406	0.65	0.13	3.16	2994
Napht$_2$[S]	380	462	0.016	0.97	<0.3	4670
Napht$_2$[Se]	389	463	<0.01	0.77	<0.3	4108

[a] Chloroform used as a solvent. [b] Quinine sulfate in aqueous H_2SO_4 0.1 M used as a reference (φ_f = 0.55). [c] Phenalenone in chloroform used as a reference (φ_Δ = 0.97). [d] TCSPC measurement, excitation source wavelength 395 nm (NanoLED), emission wavelength 450 nm.

Table 2 Calculated vertical absorption and emission energies and respective oscillator strengths at the TDDFT level in PCM/chloroform. Emission from the S_2 state is showed only for comparison of the shift

	State	E_{vert} (eV) ($S_0 \rightarrow S_n$)	f	E_{vert} (eV) ($S_n \rightarrow S_0$)	f	Stokes' shift (nm)
Napht$_2$[O]	S_1	3.86	0.911	3.35	0.942	49
	S_2	4.07	0.245	3.76	0.137	
Napht$_2$[S]	S_1	3.57	0.679	2.99	0.730	67
	S_2	3.79	0.188	3.54	0.276	
Napht$_2$[Se]	S_1	3.52	0.572	3.02	0.581	58
	S_2	3.70	0.221	3.50	0.330	

coefficient is high, *ca.* 29 000 L mol^{-1} cm^{-1}. The emission band almost mirrors the absorption, with maximum in the violet edge of the visible spectrum (λ_{em} = 405 nm). It shows a similar LE character and associated vibronic progression, with a high emission quantum yield (φ_f = 0.65).

Overall, the absorption and emission spectra of Napht$_2$[O] closely resemble those of the reference compound **NaphtOMe** (Fig. S12), exhibiting similar absorption maxima (λ_{abs} = 360 nm) and vibronic progression. The emission of **NaphtOMe** is slightly redshifted (λ_{em} = 430 nm), with the (0–2) vibronic transition becoming dominant, while the (0–1) transition remains the primary feature in **Napht$_2$[O]**. This pattern is well reproduced by the calculated spectra of the reference compound (Fig. 4). Notably, **NaphtOMe** shows a significantly higher fluorescence quantum yield (φ_f = 0.82).

Napht$_2$[S] and **Napht$_2$[Se]** show drastically different spectroscopic properties. Their UV absorption and emission spectra mainly consist of two intertwined bands, consistent with what has been recently reported for related naphthalimide dimers.[51] In both cases, a broad and structureless band appears significantly redshifted (λ_{abs} ~ 390 nm, in comparison with the maximum monitored for **Napht$_2$[O]**, which appears at 323 nm). The band tails in the visible, with an onset near 450 nm. Meanwhile, a structured band with a vibronic progression similar to that seen in **Napht$_2$[O]** is observed, but the main vibronic transition appears blueshifted to *ca.* 345 nm. Molar extinction coefficient of the broad band is significantly reduced to 22 500 and 20 000 L mol^{-1} cm^{-1} (at λ_{abs} = 390 nm) for **Napht$_2$[S]** and **Napht$_2$[Se]**, respectively. While the overlap of the two bands makes a comparison difficult, the intensity of the structured band appears much weaker in **Napht$_2$[S]** and **Napht$_2$[Se]** in comparison with **Napht$_2$[O]**.

The computed theoretical spectra exhibit features that closely resemble those observed experimentally in the absorption spectra. While **Napht$_2$[O]** shows a maximum peaked at 327 nm, **Napht$_2$[S]** and **Napht$_2$[Se]** show two partially overlapping bands (peaked at 351/312 nm for S and 355/312 nm for Se) with lower intensity compared to the oxygen analog. This characteristic band splitting (Davydov splitting),[53] along with the apparent reduction in the oscillator strength of the lowest vertical absorption (Table 2) supports the hypothesis of a pronounced intramolecular excitonic coupling,[56–59] in the systems containing sulphur and selenium, which appears to be negligible in the **Napht$_2$[O]**.

To exclude the possibility that the observed excitonic coupling arises from intermolecular aggregation, concentrated (10^{-4} M) solutions of each compound were prepared and measured by UV-vis spectroscopy. Then, spectra were recorded upon successive dilution to *ca.* 1.5 × 10^{-6} M (Fig. S13–S15). Superimposition of the spectra recorded in each case at both extremes of concentrations shows perfect overlap, which confirms that the observed effect is of a pure intramolecular nature.

As a result of this excitonic coupling process, luminescence is substantially redshifted (λ_{em} = 462 nm).[60] In the meantime,

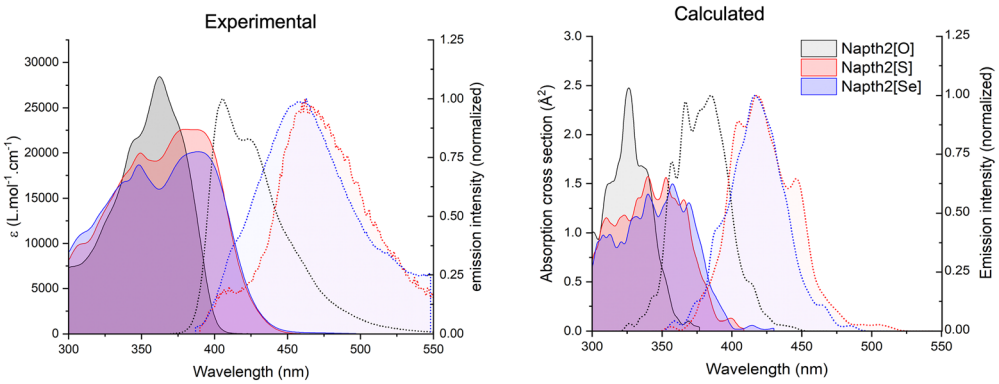

Fig. 2 Absorption (full line) and normalized emission (dashed line) spectra obtained experimentally (left) and calculated (right) for the dimers **Napht$_2$[O]** (black), **Napht$_2$[S]** (red) and **Napht$_2$[Se]** (blue).

luminescence quantum yield vanishes, dropping to 0.015 for **Napht$_2$[S]** and almost 0 for **Napht$_2$[Se]**. For the latter compound, the red edge of the spectrum reveals a weak band which, by comparison with subsequent 77 K experiments (see below), we attribute to RT phosphorescence.

Luminescence lifetime, which is 3.2 ns for **Napht$_2$[O]**, is shortened below the detection limit of our time-correlated single-photon counting (TCSPC) measurement (<0.2 ns) for the two other compounds. Altogether, this evolution suggests that strong non-radiative processes are taking place, the nature of which will be discussed in the following.

Excited state triplet phosphorescence signatures were monitored, using solutions of **Napht$_2$[Se]**, **Napht$_2$[S]**, **Napht$_2$[O]**, and **NaphtOMe** in glassy 2-methyltetrahydrofuran at 77 K. In all cases, the phosphorescence character of the band was ascertained by applying a time gate of 60 μs between the excitation and collection of the data, using the "phosphorescence" mode of our spectrofluorimeter (Fig. S16). For **Napht$_2$[S]** and **Napht$_2$[Se]**, a similar phosphorescence signature with a peak emission around 580 nm and a distinctive vibronic progression was detected. As expected, a weaker blue-shifted (*ca.* 545 nm) signal was monitored for **Napht$_2$[O]**, in line with a less effective ISC. **NaphtOMe** shows a very different spectrum, in the shape of an ill-defined 525 nm centered broad phosphorescence band of weak intensity, witnessing the very different nature of the triplet manifold in the latter.

Because the singlet and triplet excited-state emissions exhibit distinctive signatures at 77 K, it is possible to quantify their relative intensities when recording data without time gating (Fig. S17). This ratio is primarily determined by two factors: (i) the magnitude of spin–orbit coupling between the lowest-lying singlet state (S_1) and the triplet manifold at lower energies, and (ii) the radiative rate (oscillator strength) associated with the $T_1 \rightarrow S_0$ phosphorescence. Interestingly, while the emission spectrum of **Napht$_2$[O]** displays only the characteristic fluorescence signature (blue-shifted by a few nanometers relative to the RT spectrum), both fluorescence and phosphorescence bands are clearly observed for **Napht$_2$[S]**, with comparable intensities. In contrast, the 77 K spectrum of **Napht$_2$[Se]** is dominated by phosphorescence, with only a negligible residual fluorescence contribution, indicating highly efficient intersystem crossing to the triplet state and subsequent emission from T_1 at low temperature.

To estimate an approximate experimental yield for excited singlet-to-triplet intersystem crossing quantum efficiencies,[24] singlet oxygen quantum yield measurements were undertaken in chloroform (see SI, materials and methods for details, Fig. S18 for measurements). Phenalen-1-one (φ_Δ = 0.97 in chloroform) was used as a reference. While **NapthOMe** shows no significant singlet oxygen production ($\varphi_\Delta < 0.02$), a noticeable increase is seen for **Napht$_2$[O]** where φ_Δ reaches 0.13. This singlet oxygen generation quantum yield is drastically increased to 0.97 for **Napht$_2$[S]**, while **Napht$_2$[Se]** slightly drops to φ_Δ = 0.77. The faint room-temperature luminescence observed for the latter, including a participation of room-temperature phosphorescence together with the intense phosphorescence at 77 K, suggests that additional radiative and non-radiative deactivation pathways contribute to its excited-state decay. In fact, singlet oxygen generation depends not only on ISC efficiency, but also on the competition between triplet-state deactivation channels. Although **Napht$_2$[Se]** likely undergoes faster ISC because of its larger spin–orbit coupling, the same effect can also enhance phosphorescence and non-radiative triplet decay, thereby shortening the triplet lifetime available for energy transfer to oxygen. Therefore, the slightly lower Φ_Δ value of **Napht$_2$[Se]** does not indicate less efficient ISC, but rather stronger competition from intrinsic triplet-state decay pathways.

2.3. Quantum chemical calculations

Altogether, these results clearly show that intersystem crossing efficiency can be tuned by adequate coupling of these basic naphthalimide fluorophores into homomolecular dyads. To better understand the origin of this phenomenon and its dependence on the bridging chalcogen atom, we performed quantum chemical calculations at the TDDFT level for the three dimers show in Fig. 1. In all cases, we substituted the long alkyl chains with a methyl group.

The ground state minimum reveals that the two chromophore units are nearly perpendicular to each other (Fig. 3).

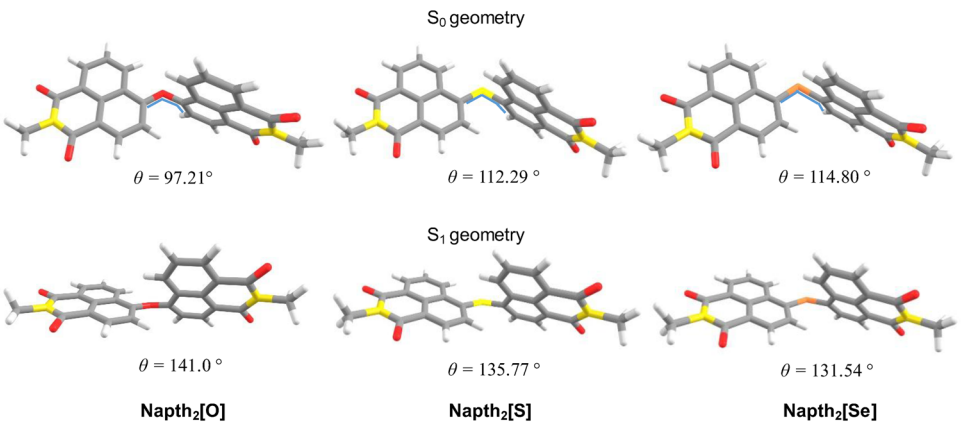

Fig. 3 Equilibrium geometries calculated for the S_0 and S_1 at the TDDFT level and central dihedral angle (in degrees) as indicated in the figure's inserts.

This observation is consistent with previous naphthalimide dimers reports exhibiting either SBCT or SOCT-ISC.[49,51] Upon relaxation to the S_1 minimum, slightly less orthogonal geometries are observed. This structural change is accompanied by a modest increase in oscillator strength for the vertical transition to the ground state. Interestingly, the dihedral change governing the relative orientation between the two counterparts of the dimer is larger for **Napht$_2$[O]** than in the sulfur and selenium analogs, which would suggest a larger Stokes shift for this compound. However, such an increase in the shift is not observed experimentally or theoretically, implying that factors beyond molecular reorganization influence the emission redshift, in agreement with our hypothesis of the excitonic nature of the transition.

The calculated lowest vertical excitations and emission are shown in Table 2, while the corresponding natural transition orbitals (NTOs) associated to the electronic transitions are shown in Fig. S19. These analyses reveal notable differences between the oxygen-based molecules and sulphur- and selenium-based analogs. While for **Napht$_2$[O]**, a strong oscillator strength is observed for the $S_0 \rightarrow S_1$ vertical excitations, the intensity of this transition is significantly reduced for the sulphur and selenium analogs. This reduction is attributed to the nature of the excited state: the NTOs for both S_1 and S_2 states for **Napht$_2$[O]** reveal that the hole and electron are localized on the same naphthalimide unit, characteristic of a local excitation. By contrast, in **Napht$_2$[S]** and **Napht$_2$[Se]**, the hole is localized on a single naphthalimide unit, and the electron is delocalized over the entire molecule, which indicates some degree of charge separation. This suggests significant electron–hole separation in S_1 of the S and Se dimers, *i.e.* a CT character. The reduced electron–hole overlap explains the lower oscillator strength of S_1 in these molecules, as CT-type excitations are less allowed, as the spatial separation reduces the electron–hole overlap.[61]

Notably, for the three dimers, the $S_0 \rightarrow S_2$ transition also exhibits significant oscillator strength, which may explain the appearance of the pronounced double peak in the absorption spectra. However, while the $S_0 \rightarrow S_2$ oscillator strength remains weak for **Napht$_2$[O]**, it markedly increases for the S and Se analogs. The analysis of the NTOs indicates that both excitations are delocalized over the whole molecule, although some degree of charge transfer character can be expected for the S_1 state of **Napht$_2$[Se]**. Interestingly, for **Napht$_2$[Se]** and **Napht$_2$[S]**, these excitations are predominantly dominated by HOMO–LUMO and HOMO–LUMO+1 transitions, whereas the S_2 state of **Napht$_2$[O]** acquires a pronounced degree of multiconfigurational character.

As already shown above, for the dimers, the simulated spectra based on a Wigner distribution[54] show similar features as the experimental spectra. These spectra include vibrational resolution and are usually redshifted in comparison to vertical excitations.[55] In Fig. 4, we show a comparison of the simulated spectra for the dimers and for their respective reference monomers. While **Napht$_2$[S]** and **Napht$_2$[Se]** show a clear splitting of the lowest-energy absorption band into two components, characteristic of a Davydov splitting, the monomers show only a single band, with their maxima overlapping with the more redshifted part of the dimer spectra. **Napht$_2$[O]**, by contrast, shows a single absorption band similar to the monomer, essentially indicating little to no excitonic character. Consequently, the dimer and monomer absorption and emission spectra for the oxygen analog have almost perfect overlapping peaks. On the other hand, for the sulphur and selenium derivatives, the emission spectra of the dimer is clearly redshifted in comparison to the monomer.

To investigate the ISC, we computed the singlet–triplet energy gap and the spin–orbit coupling (SOC)[62] values for the three molecules. As this energy gap is highly sensitive to the level of theory, we also calculated the energies at the *ab initio* CC2 level (Table S1) using geometries optimized at the TDDFT level, in order to benchmark the energy differences. Based on previously published benchmarks,[63–65] the expected standard deviation of CC2 and TD-DFT with CAM-B3LYP functional (using the Tamm–Dancoff approximation) for excited state energies is approximately 0.2 eV, while the uncertainty of CC2 for singlet–triplet gaps may be smaller than 0.1 eV. TDDFT calculations, using the CAM-B3LYP-D4 functional, which are summarized in Fig. 5, show a good agreement with the CC2 results. In all molecules, T_1 and T_2 states lie below the S_1 minimum. For **Napht$_2$[O]**, the S_1-T_2 energy gap is 1.02 eV, while for **Napht$_2$[S]** and **Napht$_2$[Se]**, the energy gap is reduced to 0.72 and 0.69 eV, respectively. At the CC2 level, these energy gaps are, respectively, 0.94, 0.66, and 0.60 eV. For these three

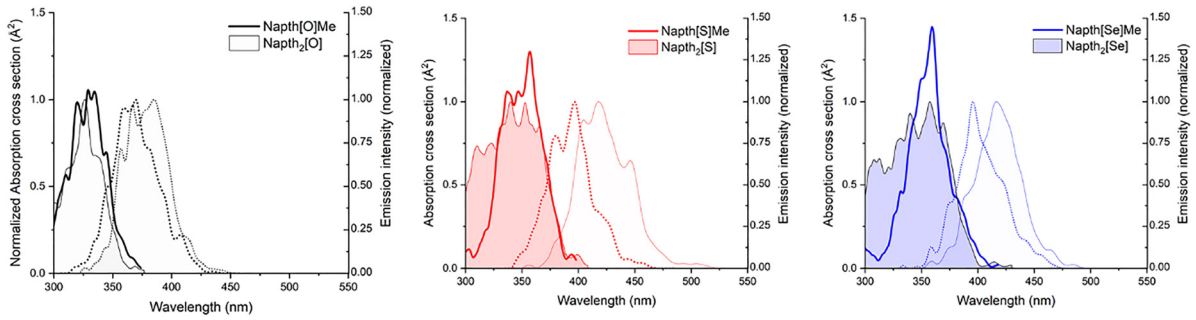

Fig. 4 Absorption (full line) and normalized emission (dashed line) spectra computed with the nuclear ensemble approach for the monomers (displayed as lines without area filling) and for the dimers (displayed with filled areas).

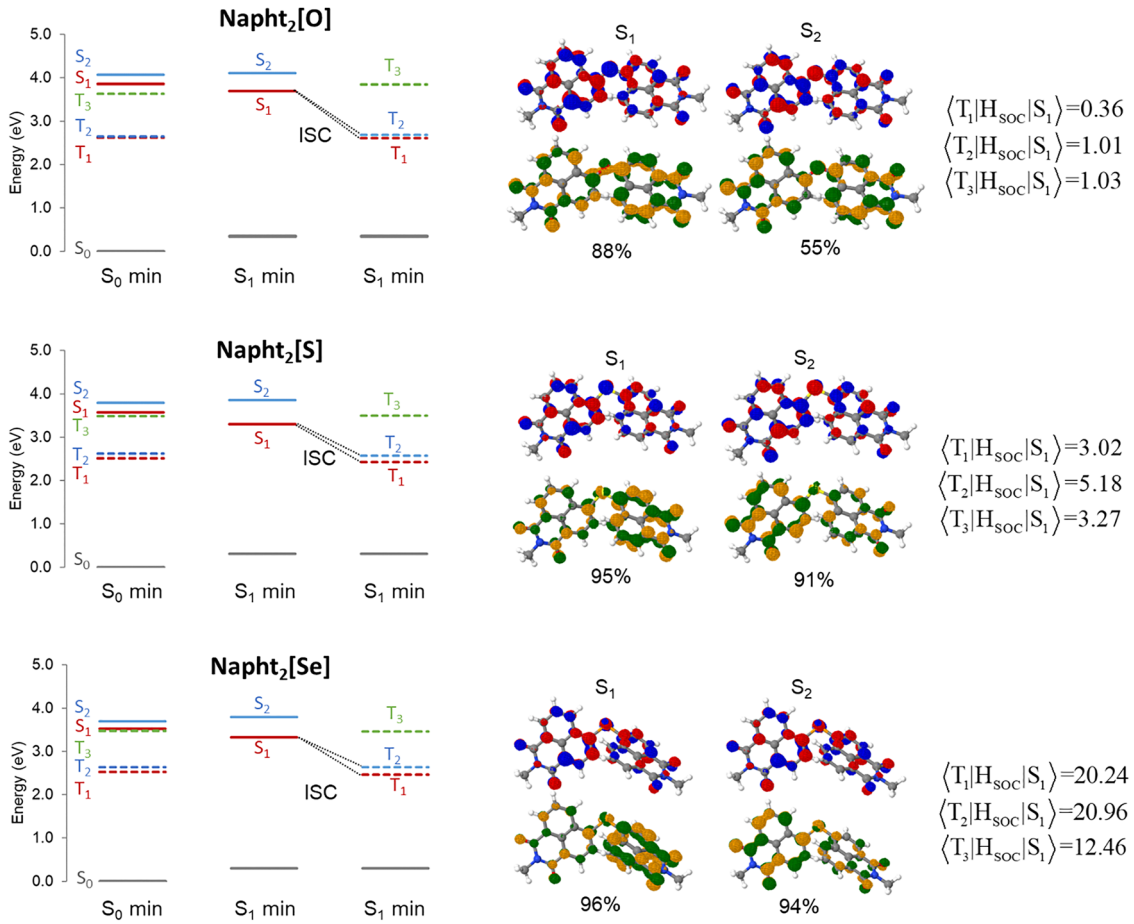

Fig. 5 (Left) Vertical energies calculated at the S_0 and S_1 minimum at the TDDFT level (left). Natural transition orbitals associated to the dominant transitions for the two lowest singlet states at the S_1 minimum (center), the bottom being the hole and the top the electron. Spin–orbit couplings, in cm^{-1}, between the S_1 and the three lowest triplet states calculated at the S_1 minimum geometry (right).

molecules, the T_3 state is also computed only slightly higher in energy than S_1 (Fig. 5 and Table S1), suggesting that this triplet state could also be involved in the ISC. In parallel, the SOC values for **Napht$_2$[O]** are found to be significantly lower than those for the sulfur and selenium analogs. Together, the reduced energy gaps and enhanced SOC values strongly suggest a more favorable ISC process in **Napht$_2$[S]** and **Napht$_2$[Se]**, consistent with experimental data.[21]

2.3.1 Accessing the dynamical nature of dimerization-induced SOC. Since the connection between the chalcogen and the two naphthalimide units is a single bond, it can freely rotate giving rise to other stable conformers that may exhibit larger SOC values. Some of us have previously shown that the molecular freedom imposed by the molecular bridge can increase SOC and remarkably enhance ISC.[52] To investigate the dependency of the SOC values with the molecular geometry, we performed a relaxed scan around the central dihedral angle for each molecule. Fig. 6 shows the relative energies and the SOC values along the rotation around this dihedral angle. Although the SOC values vary with the geometry, we observe that the S_1–T_2 coupling intensity consistently remains between 0 and 1 cm^{-1} for **Napht$_2$[O]**, between 3 and 8 cm^{-1} for **Napht$_2$[S]**, and between 15 and 35 cm^{-1} for **Napht$_2$[Se]**. The larger SOC values for the two latter explain why fluorescence quantum yield is essentially absent for these molecules. Indeed, it has been shown that, for instance, the phosphorescence-fluorescence efficiencies ratio of $\pi\pi^*$ transitions for halogenated hydrocarbons increases approximately with the square of the SOC constant.[66] Interestingly, for **Napht$_2$[S]** and **Napht$_2$[Se]**, near-orthogonal conformations exhibit a pronounced increase in SOC values, consistent with similar observations reported for other types of dimers.[52] At present, the origin of these variations is not fully understood, but they may reflect geometry-dependent selection rules or state-mixing effects governing SOC in these dimers.

Combining the effects of a smaller singlet–triplet energy gap and significantly larger SOC values observed for **Napht$_2$[S]** and **Napht$_2$[Se]** indicates that the ISC rate for these molecules should be several orders of magnitude higher than for **Napht$_2$[O]**. To definitely dismiss the possibility that the enhanced ISC is solely from the heavier-atom effect and to confirm its origin in excitonic coupling within the dimer, we calculated the singlet–triplet energy gaps and SOC values for the corresponding monomers. In these cases, one of the naphthalimide units was substituted by a methyl group (as described previously), resulting

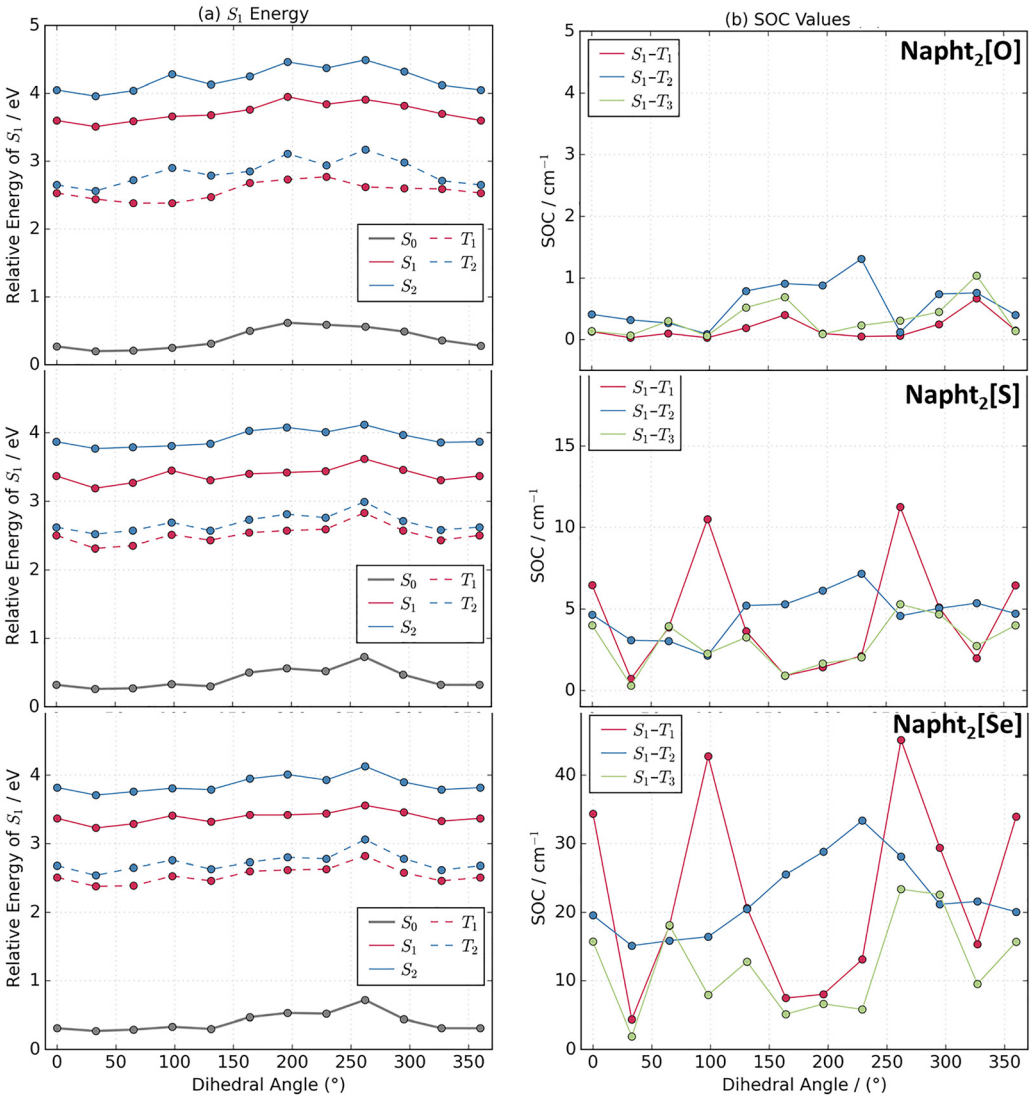

Fig. 6 Relaxed scan at the S_1 geometries: (a) relative energies between the lowest excited states and the ground state calculated along the rotation of the central dihedral angle (C–X–C–C) at the TDDFT level. (b) Respective spin–orbit couplings between S_1 and the lowest triplet states calculated along the relaxed scan.

in the reference compound **Napht[O]Me** (synthesized and studied experimentally, *vide supra*), and into **Napht[S]Me** and **Napht[Se]Me**. Vertical excitation energies and NTOs for these compounds can be seen in the SI (Table S2 and Fig. S20). Looking at the first two excitations, we observe that the $S_0 \rightarrow S_2$ transition has oscillator strengths below 0.05 in all cases, in striking contrast to the corresponding dimers. Comparing the SOC values calculated for the dimers and monomers, we observe that it vanishes in all cases (Table S3) for the monomers, reaching maximum values of 0.18 cm^{-1} for S_1–T_2 of **Napht[Se]Me**. This trend is in line with the results obtained experimentally for **Napht[O]Me**. Regarding the character of the excitations, the NTOs analysis indicates that all transitions correspond to local excitations and they are all equivalent in nature (Fig. S20).

The difference in excitation character when compared to the dimers is also evident from the electron density difference plots (Fig. S21 and S22). These results indicate that the increased ISC rates in **Napht$_2$[S]** and **Napht$_2$[Se]** cannot be attributed solely to the internal heavier-atoms, and strengthen the hypothesis that intramolecular excitonic coupling caused by dimerization plays a key role in facilitating ISC.

2.3.2 Excitonic analysis based on the transition density matrix. To further test this hypothesis and characterize the nature of the excitations in the dimers, we calculated the transition density matrix (1TDM) using the fragment-based analysis available in TheoDORE[67] program. These analyses allows for an unambiguous assignment of the excitation type, whether it corresponds to a local excitation (LE), charge transfer (CT), excitonic resonance (ER), charge resonance (CR) exciton, or a mixed ER + CR state. In this procedure, the molecule is divided into fragments (in this case, into two fragments represented in Fig. 7b): one of them contains the **Napht[X]** unit, and the other one contains the **Napht** (for the dimer) or the methyl group (for the monomer).

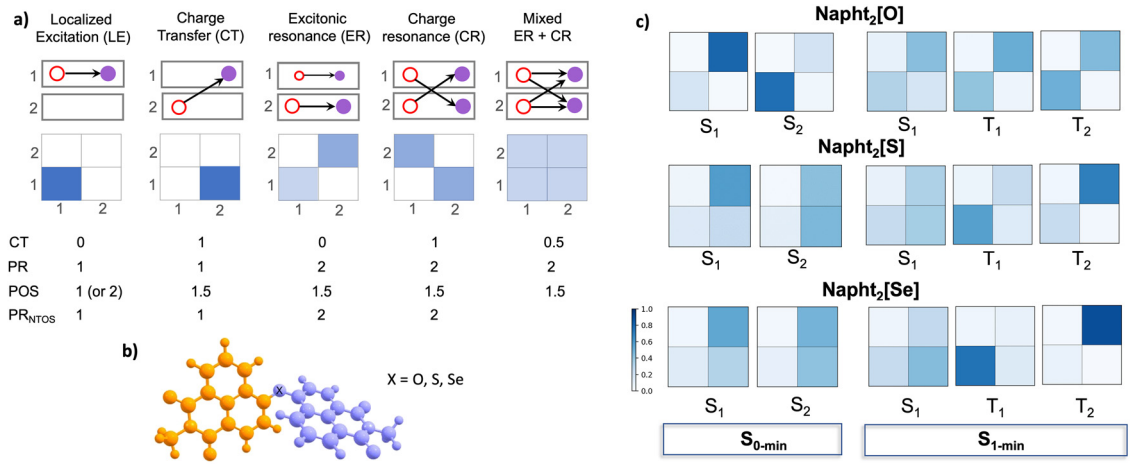

Fig. 7 (Left) Schematic representation of the different types of excited states distributed over two fragments used on the TheoDORE program. (a) Representation of the distribution of the hole (red) and electron (violet) over the fragments. (b) Molecular fragments used in the fragment-based analysis. (c) Electron–hole correlation plots of the Omega matrices for the individual states of the dimer.

Fig. 7a illustrates the different types of excitations and the main descriptors used in this work to classify them.[67,68] The white and blue squares are a graphical representation of the hole and electron population over the two fragments and are derived from the one-electron transition density matrix (1TDM) between two electronic states, the so-called Ω-matrix. From this matrix, other descriptors can also be derived: the CT number (charge transfer number), ranging from 0 (local excitation) to 1 (full charge transfer); PR (participation ratio), which stands for the exciton delocalization and indicates the number of fragments involved in the excitation (PR $\sim$ 1 indicates fairly localized states, while PR $\sim$ 2 indicates a delocalized state); POS (average position of the excitation in the dimer), where POS = 1 or POS = 2 means that the excitation is localized on either one or the other fragments, while POS = 1.5 means that the average position is between the two chromophores. Combined, these descriptors allow to identify and precise classify the nature of the excited states. A localized excitation (LE), or Frenkel exciton, is characterized by the electron–hole pair confined in the same fragment (fragment 1 in the example), while a pure charge transfer (CT) state shows the electron and the hole localized in different fragments. An excitonic resonance (ER) refers to the coherent sharing of an excitation between the two chromophores without significant charge transfer, *i.e.* the electron and hole remain in the same fragment. Charge resonance (CR), on the other hand, describes coherent mixing of CT configurations where the charge distribution between the chromophores is indistinguishable, *i.e.* when the electron and hole are on different fragments. Physically, it corresponds to a superposition of two opposite CT states (or charge resonant exciton states), where there is a partial charge separation, but overall neutrality is restored *via* resonance. Finally, a mixed ER + CT state can also be formed.

Table 3 reports the numerical values of the 1TDM descriptors. A common feature observed upon comparison with the monomer is that dimerization enables delocalization of the

Table 3 Main descriptors used to evaluate the character of the excitations. CT (charge transfer), PR (participation ratio), POS (position of the exciton in the dimer). Superscripts (0) indicate the geometry of the ground state and (1) the geometry of the first excited singlet state. *Indicates that T_2 in the monomer in higher in energy than S_1 state

		Dimer			Monomer		
		Napht$_2$[O]	**Napht$_2$[S]**	**Napht$_2$[Se]**	**Napht[O]Me**	**Napht[S]Me**	**Napht[Se]Me**
$S_1^{(0)}$	CT	0.04	0.29	0.35	0.12	0.33	0.43
	PR	1.44	1.64	1.66	1.14	1.45	1.53
	POS	1.81	1.72	1.71	1.07	1.19	1.24
$S_1^{(1)}$	CT	0.25	0.43	0.49	0.12	0.31	0.39
	PR	1.98	1.85	1.74	1.14	1.42	1.51
	POS	1.55	1.54	1.51	1.06	1.18	1.22
$T_2^{(1)}$	CT	0.06	0.07	0.04	0.08*	0.20*	0.26*
	PR	2.02	1.66	1.21	1.11	1.28	1.36
	POS	1.47	1.73	1.91	1.05	1.12	1.15
$T_1^{(1)}$	CT	0.09	0.19	0.18	0.10	0.19	0.20
	PR	2.00	1.81	1.39	1.11	1.24	1.25
	POS	1.54	1.34	1.17	1.05	1.11	1.11

excitation across the two identical fragments, an effect that becomes progressively more pronounced from O to S to Se analogs. Despite this increased delocalization, the CT number remains below 0.5, consistent with either a localized excitation or an excitonic resonance state. Additionally, a PR approaching 2 indicates that both fragments significantly contribute to the excitation, while the POS near 1.5 suggests that the exciton is symmetrically delocalized between the two units.

As illustrated in Fig. 7, the different kinds of excitations can be distinguished based on the 1TDM descriptors. Fig. 7c shows the graphical representation of the Ω-matrix for the vertical excitations (at the $S_{0\text{-min}}$) and for the S_1, T_1, and T_2 states at the S_1 optimized geometry. Starting with the **Napht$_2$[O]** dimer, one can observe that both the S_1 and S_2 vertical excitations correspond to localized excitations, which is also clearly seen in the NTOs shown in the SI Fig. S19. At the S_1 minimum, however, this state, as well as the T_1 and T_2 states, can be classified as excitonic resonance states.

The situation is markedly different for **Napht$_2$[S]** and **Napht$_2$[Se]**, which behave similarly. At the S_0 minimum, both compounds show a significant increase in the CT number for the vertical S_1 and S_2 excitations. While this increase alone may not justify classifying these states as pure CT, the presence of both partial charge separation and delocalization suggests a mixed ER + CR. Upon relaxation to the S_1 minimum, this mixed character becomes more pronounced, evolving into a clear mixed ER + CT state. Crucially, the T_2, which is the state energetically closest to S_1 and, therefore, the most accessible for the ISC, shows a different feature, with a more localized Frenkel-exciton character, particularly for the **Napht$_2$[Se]**. This change in state character between S_1 and T_2 is expected to increase the SOC, thereby enhancing the ISC. This could be seen as an analogy to the SBCT-ISC mechanism, where the required change in angular momentum is compensated by the change from a ^{1}CT to ^{3}LE state in order to promote ISC. Mixed Frenkel exciton and CT states are a hybrid that present intermediate properties, with peaks partially shifted and NTOS partially separated. The presence of mixed interactions also supports the decrease of fluorescence observed for S and Se compounds.[69]

To confirm that the enhanced ISC observed in the dimers arises from changes in excited-state character rather than simply from the presence of heavier elements (S or Se), we performed the same 1TDM-based analyses for the monomers. The results are summarized in Table 3 and in SI Fig. S24. In the monomer, fragment 1 corresponds to the Napth group (as it was for the dimer), while fragment 2 consists of the −XMe unit. For all three monomers, the T_2 state lies above S_1, indicating that ISC is likely to occur from S_1 to T_1. The descriptors reveal that **Napht[O]Me** maintains a purely localized excitation character across all relevant states. In **Napht[S]Me** and **Napht[Se]Me**, both S_1 and T_1 also exhibit predominantly local excitation character, although S_1 shows a slightly larger CT number compared to T_1. These results confirm that the enhanced ISC observed in the dimers arises from dimerization-induced changes in excited-state character between S_1 and T_2, rather than being solely due to the presence of the heavier S or Se atoms.

Overall, a clear trend is observed: the oxygen-based systems exhibit the most localized excitations, sulfur analogs show intermediate behavior, and selenium promotes the greatest electronic delocalization and CT mixing. This progression reflects the more diffuse and polarizable character of the orbitals of heavier chalcogens which may facilitate stronger coupling and charge redistribution between units.

Altogether, these results provide new evidence that tuning the inter-units electronic coupling in simple homomolecular fluorophore dyads can induce strong intramolecular excitonic couplings. In turn, such interactions offer an effective strategy to modulate intersystem crossing efficiency, demonstrating how molecular design at the fragment level can control excited-state dynamics.

Our mechanistic interpretations are based on the strong consistency between steady-state spectroscopic measurements and quantum-chemical calculations, which together support the role of excitonic coupling in promoting ISC. Nevertheless, we acknowledge that ultrafast spectroscopic investigations would be valuable to further validate and refine the proposed mechanism.

3. Conclusions

By means of nucleophilic aromatic substitutions on 4-bromo-1,8-naphthalimide derivatives, we synthesized three accessible homomolecular dyads of a naphthalimide fluorophore, simply differing by their bridging chalcogen atom (O, S, Se), and thoroughly investigated the spectroscopic and photophysical properties of these dyads experimentally and theoretically. By systematically comparing the effects of different chalcogens, we demonstrated that sulfur and selenium analogs exhibit pronounced excitonic coupling and different degrees of charge resonance, which facilitate ISC more effectively than their oxygen counterparts.

The differences in excitonic coupling behaviour translate into a marked change in the spectroscopic features of the dyads when going from **Napht$_2$[O]** to **Napht$_2$[S]** and **Napht$_2$[Se]**, with a characteristic splitting of the lowest energy transition, broadening of the red-shifted band, and redshift of the emission band. TDDFT calculations reproduce this phenomenon well and enable deeper analyses of the factors controlling the ISC in the three molecules. Examination of transition density matrices and NTOs shows that the degree of excitonic charge delocalization critically depends on the nature of the chalcogen bridge, while ruling out any isolated participation of a chalcogen-mediated heavy atom effect. As a consequence of this excitonic charge delocalization, excited singlet-to-triplet ISC is strongly favored for the third and fourth row chalcogen-bridged **Napht$_2$[S]** and **Napht$_2$[Se]**, as it can be seen by the very marked decrease in their luminescence quantum efficiency and concomitant increase in singlet oxygen generation efficiency.

Quantum chemical calculations unveiled how the dimerization-induced changes in excited-state character are crucial for

maximizing ISC rates. This detailed analysis allowed us to propose an alternate mechanism for enhancing ISC in organic dimers when compared to typical SBCT-ISC pathways documented in the literature. In **Napht$_2$[O]**, S_1 and S_2 are essentially localized excitations with minimal inter-unit coupling, whereas in **Napht$_2$[S]** and **Napht$_2$[Se]**, S_1 becomes a delocalized excitonic state with partial CT character, and S_2 acquires a more localized character. Importantly, no long-lived full charge-separated state was observed in these dimers; instead, the S_1 state itself has a mixed excitonic and charge resonance character.

In contrast with SOCT-ISC and SBCT-ISC mechanisms, where ISC is associated with the formation of a full charge-separated state arising from the near orthogonal orientation between donor and acceptor, our proposed mechanism does not require a long-lived fully charge-separated intermediate. Instead, a strong electronic coupling between the two chromophore units generates mixed excited states with combined excitonic-resonance and partial CT character. Changes in the nature of the interacting singlet and triplet states are accompanied by changes in molecular orbital momentum, which increases spin–orbit coupling and promotes ISC. Thus, while SOCT-ISC and SBCT-ISC are primarily driven by charge separation/recombination dynamics, the present mechanism is better described as coupling-induced state mixing ISC (CISM-ISC) within an exciton manifold. It provides an alternative framework for understanding ISC enhancement in compact homodimers where complete charge separation is energetically unfavorable or not experimentally observed.

In summary, we demonstrated that by increasing exciton coupling through heavier chalcogen bridges, one can dramatically accelerate ISC in such homodimers by inducing a change in the character between the excited singlet and triplet state, without invoking a full charge separation step. This study further unveils the role of excitonic coupling in the obtention of large spin–orbit coupling, and makes the evaluation of the magnitude of the latter a powerful predictive computational tool for the assessment of the potential of a given dyad compound for triplet harvesting and singlet oxygen generation.

Author contributions

Conceptualization: MGM, YZ, CM; data curation: AHGD, DPS, CC, JMT, CM; formal analysis: MGM, JMT, AHGD, DPS, CC, CM; funding acquisition: YZ, CC, CM, JMT, TLB; investigation: MGM, CM, JMT; methodology: AHGD, CM, CC, JMT, TLB; project administration: YZ, CC, CM, JMT; resources: YZ, CC, CM, TLB, JMT; supervision: YZ, CC, CM; validation: CM, JMT; visualization: CM, JMT; writing – original draft: YZ, CM, JMT; writing – review & editing: all authors.

Conflicts of interest

There are no conflicts to declare.

Data availability

The data that support the findings of this study will be openly available at a Zenodo repository DOI: https://doi.org/10.5281/zenodo.18761180.

Supplementary information (SI) is available. See DOI: https://doi.org/10.1039/d6cp00935b.

Acknowledgements

We gratefully acknowledge support from the CBPsmn (PSMN, Pôle Scientifique de Modélisation Numérique) of the ENS de Lyon for the computing resources (the platform operates the SIDUS solution) [E. Quemener and M. Corvellec, Linux J., 2013, 2013, 3.]. JMT acknowledges the access granted to the HPC resources of TGCC under the allocation A0170800609 made by GENCI, Lyon1 University for the funding provided through AAP Accueil EC, and the French National Research Agency under project ANR-25-CE29-2684-01 (SupraPhoMo). MM and YZ would like to acknowledge the European Union-NextGenerationEU through the National Recovery and Resilience Plan of the Republic of Bulgaria, project no. BG-RRP-2.004-0008 and Bulgarian National Science Fund by grant number KP-06-H69/1.

References

1 L. Geng, R. Sun, D.-S. Zhang, M.-H. Yu, Z. Chang and X.-H. Bu, Harnessing triplet excitons: Advances in luminescence metal coordination compounds, *Coord. Chem. Rev.*, 2024, **518**, 216066.
2 S. Datta and J. Xu, Recent Advances in Organic Molecular-to-Supramolecular Self-Assembled Room-Temperature Phosphorescent Materials for Biomedical Applications, *ACS Appl. Bio Mater.*, 2023, **6**(11), 4572.
3 J. Dai, X. Wu, S. Ding, X. Lou, F. Xia, S. Wang and Y. Hong, Aggregation-Induced Emission Photosensitizers: From Molecular Design to Photodynamic Therapy, *J. Med. Chem.*, 2020, **63**(5), 1996.
4 S. E. Seo, H.-S. Choe, H. Cho, H.-I. Kim, J.-H. Kim and O. S. Kwon, Recent advances in materials for and applications of triplet–triplet annihilation-based upconversion, *J. Mater. Chem. C*, 2022, **10**(12), 4483.
5 V. W.-W. Yam, Using synthesis to steer excited states and their properties and functions, *Nature Synthesis*, 2023, **2**(2), 94.
6 X. Zhang, Y. Hou, X. Xiao, X. Chen, M. Hu, X. Geng, Z. Wang and J. Zhao, Recent development of the transition metal complexes showing strong absorption of visible light and long-lived triplet excited state: From molecular structure design to photophysical properties and applications, *Coord. Chem. Rev.*, 2020, **417**, 213371.
7 H. Yersin, A. F. Rausch, R. Czerwieniec, T. Hofbeck and T. Fischer, The triplet state of organo-transition metal compounds. Triplet harvesting and singlet harvesting for efficient OLEDs, *Coord. Chem. Rev.*, 2011, **255**(21), 2622.

8 Q. Wei, N. Fei, A. Islam, T. Lei, L. Hong, R. Peng, X. Fan, L. Chen, P. Gao and Z. Ge, Small-Molecule Emitters with High Quantum Efficiency: Mechanisms, Structures, and Applications in OLED Devices, *Adv. Opt. Mater.*, 2018, **6**(20), 1800512.
9 D. Chen, W. Li, L. Gan, Z. Wang, M. Li and S.-J. Su, Non-noble-metal-based organic emitters for OLED applications, *Mater. Sci. Eng. R Rep.*, 2020, **142**, 100581.
10 S. Fukuzumi, K. Ohkubo and T. Suenobu, Long-Lived Charge Separation and Applications in Artificial Photosynthesis, *Acc. Chem. Res.*, 2014, **47**(5), 1455.
11 P. D. Frischmann, K. Mahata and F. Würthner, Powering the future of molecular artificial photosynthesis with light-harvesting metallosupramolecular dye assemblies, *Chem. Soc. Rev.*, 2013, **42**(4), 1847.
12 X. Zhao, Y. Hou, L. Liu and J. Zhao, Triplet Photosensitizers Showing Strong Absorption of Visible Light and Long-Lived Triplet Excited States and Application in Photocatalysis: A Mini Review, *Energy Fuels*, 2021, **35**(23), 18942.
13 J. Großkopf, T. Kratz, T. Rigotti and T. Bach, Enantioselective Photochemical Reactions Enabled by Triplet Energy Transfer, *Chem. Rev.*, 2022, **122**(2), 1626.
14 Y.-M. Lee, W. Nam and S. Fukuzumi, Redox catalysis via photoinduced electron transfer, *Chem. Sci.*, 2023, **14**(16), 4205.
15 H. Kumagai, Y. Tamaki and O. Ishitani, Photocatalytic Systems for CO2 Reduction: Metal-Complex Photocatalysts and Their Hybrids with Photofunctional Solid Materials, *Acc. Chem. Res.*, 2022, **55**(7), 978.
16 P. R. Ogilby, Singlet oxygen: there is still something new under the sun, and it is better than ever, *Photochem. Photobiol. Sci.*, 2010, **9**(12), 1543.
17 A. Greer, Christopher Foote's Discovery of the Role of Singlet Oxygen [1O2 (1Δg)] in Photosensitized Oxidation Reactions, *Acc. Chem. Res.*, 2006, **39**(11), 797.
18 I. Pibiri, S. Buscemi, A. Palumbo Piccionello and A. Pace, Photochemically Produced Singlet Oxygen: Applications and Perspectives, *ChemPhotoChem*, 2018, **2**(7), 535.
19 C. M. Marian, Understanding and Controlling Intersystem Crossing in Molecules, *Annu. Rev. Phys. Chem.*, 2021, **72**, 617.
20 D. Sasikumar, A. T. John, J. Sunny and M. Hariharan, Access to the triplet excited states of organic chromophores, *Chem. Soc. Rev.*, 2020, **49**(17), 6122.
21 C. M. Marian, *In Reviews in Computational Chemistry*, ed Lipkowitz, K. B.; Boyd, D. B., 2001.
22 S. P. McGlynn, J. Daigre and F. J. Smith, External Heavy-Atom Spin—Orbital Coupling Effect. IV. Intersystem Crossing, *J. Chem. Phys.*, 1963, **39**(3), 675.
23 X. Cui, J. Zhao, Z. Mohmood and C. Zhang, Accessing the Long-Lived Triplet Excited States in Transition-Metal Complexes: Molecular Design Rationales and Applications, *Chem. Rec.*, 2016, **16**(1), 173.
24 B. Mettra, Y. Y. Liao, T. Gallavardin, C. Armagnat, D. Pitrat, P. Baldeck, T. Le Bahers, C. Monnereau and C. Andraud, A combined theoretical and experimental investigation on the influence of the bromine substitution pattern on the photophysics of conjugated organic chromophores, *Phys. Chem. Chem. Phys.*, 2018, **20**(5), 3768.
25 X. Hao, W. Feng, Y. Tang, X. Mu, Y. Zhao, Y. Lu and X. Zhou, Decoding the heavy atom effect and Spin–orbit coupling in D-A Molecules: Synergy or Antagonism in facilitating intersystem crossing, *Dyes Pigm.*, 2025, **242**, 112951.
26 S. Lower and M. El-Sayed, The triplet state and molecular electronic processes in organic molecules, *Chem. Rev.*, 1966, **66**(2), 199.
27 M. Deiana, P. Josse, C. Dalinot, A. Osmolovskyi, P. S. Marqués, J. M. A. Castán, L. Abad Galán, M. Allain, L. Khrouz and O. Maury, *et al.*, Site-selected thionated benzothioxanthene chromophores as heavy-atom-free small-molecule photosensitizers for photodynamic therapy, *Commun. Chem.*, 2022, **5**(1), 142.
28 M. Alías-Rodríguez, C. de Graaf and M. Huix-Rotllant, Ultrafast Intersystem Crossing in Xanthone from Wavepacket Dynamics, *J. Am. Chem. Soc.*, 2021, **143**(51), 21474.
29 R. Kumar, H. Aggarwal and A. Srivastava, Of Twists and Curves: Electronics, Photophysics, and Upcoming Applications of Non-Planar Conjugated Organic Molecules, *Chem. – Eur. J.*, 2020, **26**(47), 10653.
30 X. Zhang, Z. Wang, Y. Hou, Y. Yan, J. Zhao and B. Dick, Recent development of heavy-atom-free triplet photosensitizers: molecular structure design, photophysics and application, *J. Mater. Chem. C*, 2021, **9**(36), 11944.
31 V.-N. Nguyen, Y. Yan, J. Zhao and J. Yoon, Heavy-Atom-Free Photosensitizers: From Molecular Design to Applications in the Photodynamic Therapy of Cancer, *Acc. Chem. Res.*, 2021, **54**(1), 207.
32 M. Deiana, A. Castán, M. José, P. Josse, A. Kahsay, D. P. Sánchez, K. Morice, N. Gillet, R. Ravindranath, A. K. Patel and P. Sengupta, *et al.*, A new G-quadruplex-specific photosensitizer inducing genome instability in cancer cells by triggering oxidative DNA damage and impeding replication fork progression, *Nucleic Acids Res.*, 2023, **51**(12), 6264.
33 D. Puchán Sánchez, P. Josse, N. Plassais, G. Park, Y. Khan, Y. Park, M. Seinfeld, A. Guyard, M. Allain and F. Gohier, *et al.*, Driving Triplet State Population in Benzothioxanthene Imide Dyes: Let's twist!, *Chem. – Eur. J.*, 2024, **30**(27), e202400191.
34 L. A. Galán, J. M. Andrés Castán, C. Dalinot, P. S. Marqués, P. Blanchard, O. Maury, C. Cabanetos, T. Le Bahers and C. Monnereau, Theoretical and experimental investigation on the intersystem crossing kinetics in benzothioxanthene imide luminophores, and their dependence on substituent effects, *Phys. Chem. Chem. Phys.*, 2020, **22**(22), 12373.
35 J. Zhao, K. Chen, Y. Hou, Y. Che, L. Liu and D. Jia, Recent progress in heavy atom-free organic compounds showing unexpected intersystem crossing (ISC) ability, *Org. Biomol. Chem.*, 2018, **16**(20), 3692.
36 I. García-Moreno, V. Postils, E. Rebollar, M. J. Ortiz, A. R. Agarrabeitia and D. Casanova, Generation of multiple triplet states in an orthogonal bodipy dimer: a breakthrough spectroscopic and theoretical approach, *Phys. Chem. Chem. Phys.*, 2022, **24**(10), 5929.

37 Z. Wang, L. Ma, H. Zhao, Y. Wan, X.-F. Zhang, Y. Li, Z. Kuang and A. Xia, Spin–orbit charge-transfer intersystem crossing in heavy-atom-free orthogonal covalent boron-dipyrromethene heterodimers, *Phys. Chem. Chem. Phys.*, 2023, **25**(36), 24386.

38 Y. E. Kandrashkin, Z. Wang, A. A. Sukhanov, Y. Hou, X. Zhang, Y. Liu, V. K. Voronkova and J. Zhao, Balance between triplet states in photoexcited orthogonal BODIPY dimers, *J. Phys. Chem. Lett.*, 2019, **10**(15), 4157.

39 Y. Liu, J. Zhao, A. Iagatti, L. Bussotti, P. Foggi, E. Castellucci, M. Di Donato and K.-L. Han, A Revisit to the Orthogonal Bodipy Dimers: Experimental Evidence for the Symmetry Breaking Charge Transfer-Induced Intersystem Crossing, *J. Phys. Chem. C*, 2018, **122**(5), 2502.

40 Z. Wang, M. Ivanov, Y. Gao, L. Bussotti, P. Foggi, H. Zhang, N. Russo, B. Dick, J. Zhao and M. Di Donato, Spin–Orbit Charge-Transfer Intersystem Crossing (ISC) in Compact Electron Donor–Acceptor Dyads: ISC Mechanism and Application as Novel and Potent Photodynamic Therapy Reagents, *Chem. – Eur. J.*, 2020, **26**(5), 1091.

41 Y. Dong, A. Elmali, J. Zhao, B. Dick and A. Karatay, Long-Lived Triplet Excited State Accessed with Spin–Orbit Charge Transfer Intersystem Crossing in Red Light-Absorbing Phenoxazine-Styryl BODIPY Electron Donor/Acceptor Dyads, *ChemPhysChem*, 2020, **21**(13), 1388.

42 X. Chen, N. Rehmat, I. V. Kurganskii, P. Maity, A. Elmali, J. Zhao, A. Karatay, O. F. Mohammed and M. V. Fedin, Efficient Spin–Orbit Charge-Transfer Intersystem Crossing and Slow Intramolecular Triplet–Triplet Energy Transfer in Bodipy–Perylenebisimide Compact Dyads and Triads, *Chem. – Eur. J.*, 2023, **29**(61), e202302137.

43 T. Mikulchyk, S. Karuthedath, C. S. P. De Castro, A. A. Buglak, A. Sheehan, A. Wieder, F. Laquai, I. Naydenova and M. A. Filatov, Charge transfer mediated triplet excited state formation in donor–acceptor–donor BODIPY: Application for recording of holographic structures in photopolymerizable glass, *J. Mater. Chem. C*, 2022, **10**(32), 11588.

44 M. A. Filatov, Heavy-atom-free BODIPY photosensitizers with intersystem crossing mediated by intramolecular photoinduced electron transfer, *Org. Biomol. Chem.*, 2020, **18**(1), 10.

45 E. Bassan, A. Gualandi, P. G. Cozzi and P. Ceroni, Design of BODIPY dyes as triplet photosensitizers: electronic properties tailored for solar energy conversion, photoredox catalysis and photodynamic therapy, *Chem. Sci.*, 2021, **12**(19), 6607.

46 Y. Dong, M. Taddei, S. Doria, L. Bussotti, J. Zhao, G. Mazzone and M. Di Donato, Torsion-Induced Nonradiative Relaxation of the Singlet Excited State of meso-Thienyl Bodipy and Charge Separation, Charge Recombination-Induced Intersystem Crossing in Its Compact Electron Donor/Acceptor Dyads, *J. Phys. Chem. B*, 2021, **125**(18), 4779.

47 Z. Wang, M. Ivanov, Y. Gao, L. Bussotti, P. Foggi, H. Zhang, N. Russo, B. Dick, J. Zhao and M. Di Donato, *et al.*, Spin–Orbit Charge-Transfer Intersystem Crossing (ISC) in Compact Electron Donor–Acceptor Dyads: ISC Mechanism and Application as Novel and Potent Photodynamic Therapy Reagents, *Chem. – Eur. J.*, 2020, **26**(5), 1091.

48 M. T. Whited, N. M. Patel, S. T. Roberts, K. Allen, P. I. Djurovich, S. E. Bradforth and M. E. Thompson, Symmetry-breaking intramolecular charge transfer in the excited state of meso-linked BODIPY dyads, *Chem. Commun.*, 2012, **48**(2), 284.

49 R. Jing, Y. Li, K. Tajima, Y. Wan, N. Fukui, H. Shinokubo, Z. Kuang and A. Xia, Excimer Formation Driven by Excited-State Structural Relaxation in a Covalent Aminonaphthalimide Dimer, *J. Phys. Chem. Lett.*, 2024, **15**(5), 1469.

50 H. Song, H. Zhao, Y. Guo, A. M. Philip, Q. Guo, M. Hariharan and A. Xia, Distinct Excited-State Dynamics of Near-Orthogonal Perylenimide Dimer: Conformational Planarization versus Symmetry Breaking Charge Transfer, *J. Phys. Chem. C*, 2020, **124**(1), 237.

51 W. Tian, A. A. Sukhanov, L. Bussotti, J. Pang, J. Zhao, V. K. Voronkova, M. Di Donato and M.-D. Li, Charge Separation and Intersystem Crossing in Homo- and Hetero-Compact Naphthalimide Dimers, *J. Phys. Chem. B*, 2022, **126**(23), 4364.

52 L. A. Galán, J. M. Andrés Castán, C. Dalinot, P. S. Marqués, J. Galiana, P. Blanchard, C. Andraud, E. Dumont, O. Maury and C. Cabanetos, *et al.*, Exploring the Concept of Dimerization-Induced Intersystem Crossing: At the Origins of Spin–Orbit Coupling Selection Rules, *J. Phys. Chem. B*, 2021, **125**(30), 8572.

53 D. Abramavicius, B. Palmieri, D. V. Voronine, F. Šanda and S. Mukamel, Coherent Multidimensional Optical Spectroscopy of Excitons in Molecular Aggregates; Quasiparticle versus Supermolecule Perspectives, *Chem. Rev.*, 2009, **109**(6), 2350.

54 R. Crespo-Otero and M. Barbatti, Spectrum simulation and decomposition with nuclear ensemble: formal derivation and application to benzene, furan and 2-phenylfuran, *Theor. Chem. Acc.*, 2012, **131**(6), 1237.

55 S. Bai, R. Mansour, L. Stojanović, J. M. Toldo and M. Barbatti, On the origin of the shift between vertical excitation and band maximum in molecular photoabsorption, *J. Mol. Model.*, 2020, **26**(5), 107.

56 N. J. Hestand and F. C. Spano, Expanded Theory of H- and J-Molecular Aggregates: The Effects of Vibronic Coupling and Intermolecular Charge Transfer, *Chem. Rev.*, 2018, **118**(15), 7069.

57 M. P. Lijina, A. Benny, E. Sebastian and M. Hariharan, Keeping the chromophores crossed: evidence for null exciton splitting, *Chem. Soc. Rev.*, 2023, **52**(19), 6664.

58 T. Maeda, T. V. Nguyen, Y. Kuwano, X. Chen, K. Miyanaga, H. Nakazumi, S. Yagi, S. Soman and A. Ajayaghosh, Intramolecular Exciton-Coupled Squaraine Dyes for Dye-Sensitized Solar Cells, *J. Phys. Chem. C*, 2018, **122**(38), 21745.

59 X. Guo, J. Yang, M. Li, F. Zhang, W. Bu, H. Li, Q. Wu, D. Yin, L. Jiao and E. Hao, Unique Double Intramolecular and Intermolecular Exciton Coupling in Ethene-Bridged aza-BODIPY Dimers for High-Efficiency Near-Infrared Photothermal Conversion and Therapy, *Angew. Chem., Int. Ed.*, 2022, **61**(44), e202211081.

60 N. J. Hestand and F. C. Spano, Molecular Aggregate Photophysics beyond the Kasha Model: Novel Design Principles for Organic Materials, *Acc. Chem. Res.*, 2017, **50**(2), 341.

61 A. W. Lange and J. M. Herbert, Both Intra- and Interstrand Charge-Transfer Excited States in Aqueous B-DNA Are Present at Energies Comparable To, or Just Above, the 1ππ* Excitonic Bright States, *J. Am. Chem. Soc.*, 2009, **131**(11), 3913.

62 B. de Souza, G. Farias, F. Neese and R. Izsák, Predicting Phosphorescence Rates of Light Organic Molecules Using Time-Dependent Density Functional Theory and the Path Integral Approach to Dynamics, *J. Chem. Theory Comput.*, 2019, **15**(3), 1896.

63 I. Knysh, F. Lipparini, A. Blondel, I. Duchemin, X. Blase, P.-F. Loos and D. Jacquemin, Reference CC3 Excitation Energies for Organic Chromophores: Benchmarking TD-DFT, BSE/GW, and Wave Function Methods, *J. Chem. Theory Comput.*, 2024, **20**(18), 8152.

64 P.-F. Loos, M. Boggio-Pasqua, A. Blondel, F. Lipparini and D. Jacquemin, QUEST Database of Highly-Accurate Excitation Energies, *J. Chem. Theory Comput.*, 2025, **21**(16), 8010.

65 P.-F. Loos, F. Lipparini and D. Jacquemin, Heptazine, Cyclazine, and Related Compounds: Chemically-Accurate Estimates of the Inverted Singlet–Triplet Gap, *J. Phys. Chem. Lett.*, 2023, **14**(49), 11069.

66 D. S. McClure, Triplet-Singlet Transitions in Organic Molecules. Lifetime Measurements of the Triplet State, *J. Chem. Phys.*, 1949, **17**(10), 905.

67 F. Plasser, TheoDORE: A toolbox for a detailed and automated analysis of electronic excited state computations, *J. Chem. Phys.*, 2020, **152**(8), 084108.

68 F. Plasser and H. Lischka, Analysis of Excitonic and Charge Transfer Interactions from Quantum Chemical Calculations, *J. Chem. Theory Comput.*, 2012, **8**(8), 2777.

69 Y. J. Bae, D. Shimizu, J. D. Schultz, G. Kang, J. Zhou, G. C. Schatz, A. Osuka and M. R. Wasielewski, Balancing Charge Transfer and Frenkel Exciton Coupling Leads to Excimer Formation in Molecular Dimers: Implications for Singlet Fission, *J. Phys. Chem. A*, 2020, **124**(41), 8478.

